Lipid-Coated Nanodrops and Microbubbles

Mark A. Borden

Contents

Abstract

Lipid-coated microbubbles and nanodrops are used in many applications of biomedical ultrasound. They serve as ultrasound contrast agents, molecular imaging probes, targeted drug delivery vehicles, nucleic acid vectors, gas carriers, and enhancers of thermal ablation. Each application has a unique set of performance criteria – there is no "one size fits all" microbubble formulation. Rational design can be accomplished using the composition → processing → structure → property → performance paradigm first described by DH Kim for lipid-coated

M.A. Borden (✉)
Department of Mechanical Engineering, University of Colorado, Boulder, CO, USA
e-mail: mark.borden@colorado.edu

M. Ashokkumar (ed.), *Handbook of Ultrasonics and Sonochemistry*,
DOI 10.1007/978-981-287-278-4_26

microbubbles over a decade ago. One notable example has been the synthesis of longer circulating microbubbles through centrifugal isolation of larger diameter microbubbles coated with long acyl chain phospholipids. The purpose of this chapter is to inform the reader of current knowledge of the effects of lipid composition and processing on microstructure, as well as the effects of microstructure on important physical properties, such as microbubble size and shell viscoelasticity. More research is necessary to further elucidate these interrelationships and to exploit them for innovative microbubble designs.

Keywords
Lipid-coated microbubbles • Rational design • Nanodrop fabrication

Introduction

The lipid monolayer is nature's solution to the problem of stabilizing a gas/water interface. The most prominent example is the lung: phospholipid is the main component of lung surfactant, which stabilizes the lung alveoli by reducing surface tension and providing mechanical rigidity [1]. Premature infants born without functional surfactant are unable to breathe properly and suffer from acute respiratory distress syndrome (ARDS). The treatment for neonatal ARDS is surfactant therapy, in which animal-derived and lipid-fortified surfactant is aspirated into the patient's lung. Another example is the eye: a lipid membrane coats and stabilizes the aqueous tear film against evaporation and rupture [2]. Dysfunction in the lipid layer of the eye can lead to ocular disease, such as dry eye. Lipids synthesized by specialized cells and excreted into the aqueous subphase spontaneously assemble into a monolayer at the air/water interface to provide these functions. It is therefore not surprising that scientists and engineers have utilized the lipid monolayer as an ideal self-assembling biomaterial to stabilize microbubbles and nanodrops used for applications in ultrasonics.

Lipid-coated microbubbles (1–10 μm) are used as echogenic contrast agents to illuminate the blood compartment on the ultrasound video screen [3–5]. Without microbubbles, the presence of blood is obscured by tissue scatter. When microbubbles are injected intravenously, the vascular structures and perfused tissue suddenly light up. The brightness on the video screen comes from the strong scattering amplitude of the microbubble. Microbubbles have a gas core that is highly compressible and pulsates with the passage of each mechanical acoustic wave. In fact, microbubbles resonate when driven at acoustic frequencies used by common diagnostic imaging scanners (1–10 MHz). Each microbubble is like a tiny bell, and modern ultrasound scanners employ specific pulse sequences to filter out the echo of each microbubble based on its peculiar tone. This has enabled enhanced ultrasound imaging of the blood pool in cardiology and radiology [6, 7], and more recently there has been a strong interest in ultrasound molecular imaging to assess the physiology of diseased vasculature [8]. Currently, a vast majority of the ultrasound contrast agents approved for clinical use are lipid-coated microbubbles.

Microbubbles are used also in ultrasound therapy. The response of a microbubble to ultrasound transitions from ringing (stable cavitation) to banging (inertial cavitation) as the acoustic intensity is increased. Inertial cavitation can be used to open up pores in the vasculature that allow drugs to move from the blood pool to the tissue compartment. Thus, the interaction of microbubbles with focused ultrasound allows one to manipulate the pharmacodynamics of a drug with excellent temporal and spatial control by virtue of when and where one points the acoustic focus. Additionally, the microbubble can be engineered to carry a drug payload that is simultaneously released with the opening of the vasculature [9]. Ultimately, the imaging and therapy functions of microbubbles can be combined for theranostic applications, such as image-guided cancer therapy.

The rich variety of ultrasonics applications that employ microbubbles calls for rational design, so that a specific microbubble formulation can be tailored to a particular use (Fig. 1). Dennis Heejong Kim, a student of David Needham at Duke University, first pioneered a set of design rules for lipid-coated microbubbles based on the general material science paradigm of composition → processing → structure → property → performance [10]. DH Kim first showed how lipid acyl chain length could be varied to control the surface shear properties of the monolayer film that coats each microbubble. He then went on to show that processing affects microstructure, which in turn controls the surface shear properties. Subsequent research has gone on to validate this approach by showing how other properties of the lipid shell, such as gas permeability and surface dilatational elasticity, as well as biomedical performance, depend on lipid composition and microstructure. The goal of this chapter is to provide the interested reader with an overview of this rational design paradigm for lipid-coated microbubbles and nanodrops.

Microbubble Composition

Uncoated Microbubbles Are Unstable

At the most basic level, a microbubble is simply a 1–10-μm-diameter gas sphere suspended in an aqueous medium. However, there is tension (σ) at the gas/water interface, and, owing to the spherical geometry, a pressure jump exists across the interface (Laplace pressure) [11]:

$$P_b - P_0 = \frac{2\sigma}{R} \tag{1}$$

where P_b is the pressure inside the bubble, P_0 is the hydrostatic pressure of the aqueous medium surrounding the bubble, and R is the bubble radius. For a 1.0-μm-diameter air bubble in water ($\sigma = 73\text{mN/m}$), the pressure inside the bubble is ~0.3 MPa greater than the surrounding medium. Thus, the gas molecules in the bubble have a much higher fugacity than those dissolved in the surrounding medium [12]. This sets up a chemical potential gradient that drives mass flux from the

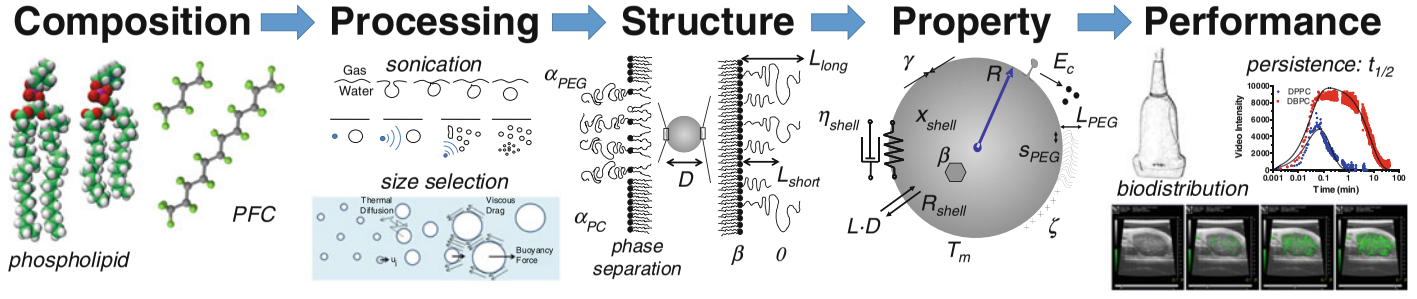

Fig. 1 Rational design of lipid-coated microbubbles. DH Kim first demonstrated the utility of employing the composition → processing → structure → property → performance paradigm to engineering lipid-coated microbubbles [10]. Research continues today to establish key structure–property–performance relationships for enhanced biomedical performance

microbubble – the microbubble is thermodynamically unstable. The rate of dissolution can be modeled by the Epstein–Plesset equation [13]:

$$-\frac{dR}{dt} = \frac{LD}{R}\left(\frac{1 + 2\sigma/P_0R - f}{1 + 4\sigma/3P_0R}\right) \tag{2}$$

where L is the Ostwald coefficient for the gas solubility, D is the gas diffusivity in water, and f is the solubility fraction of the gas in water. Equation 2 neglects the time to set up the concentration boundary layer, as this is very fast compared to the bubble wall velocity [14]. Epstein and Plesset's model predicts that, even when the aqueous solution is saturated with gas ($f = 1$) at hydrostatic pressure P_0, the Laplace pressure drives very rapid dissolution. Equation 2 predicts that a 1.0-μm-diameter air bubble in water dissolves within three milliseconds (Fig. 2). One may use less soluble gases to enhance stability. However, even perfluorobutane, which has a permeation coefficient (LD) ~300 times lower than that of air, cannot stabilize an uncoated microbubble for more than a minute [9]. Therefore, one may conclude that the uncoated microbubble is both thermodynamically and kinetically unstable.

The Lipid/PEG-Lipid Coating Provides Metastability

Needham et al. argued that a lipid monolayer coating between the gas and water phases effectively eliminates tension in the interface ($\sigma = 0$) in order to explain the "indefinite" persistence of lipid-coated air microbubbles in air-saturated aqueous media [14, 15]. Borden et al. initially disputed this claim, as the same lipid monolayers on the Langmuir trough were found to collapse at surface tensions well above zero [16]. However, it was later revealed by Witten et al. that the Wilhelmy plate method used with the Langmuir trough becomes inaccurate at very low surface tensions [17]; the method assumes the monolayer is a liquid with an isotropic stress distribution, but highly compressed lipid monolayers can act as solid elastic membranes with an anisotropic stress distribution, leading to artifacts in the measurement. The observation that most microbubbles are spherical under the microscope suggests that the lipid monolayer has some tension. One can estimate a lower limit for the surface tension by use of the Bond number (Bo), which is a ratio of the buoyant to surface tension forces:

$$Bo = \frac{\Delta\rho g R^2}{\sigma} \tag{3}$$

where $\Delta\rho$ is the density difference between the gas and aqueous phases and g is gravitational acceleration. The buoyancy force flattens the bubble out against the surface above, while the surface tension force contracts the bubble into a sphere. The fact that a resting lipid-coated microbubble is observed to be a sphere suggests that the Bond number is less than unity, and therefore the lower limit of the surface tension must be:

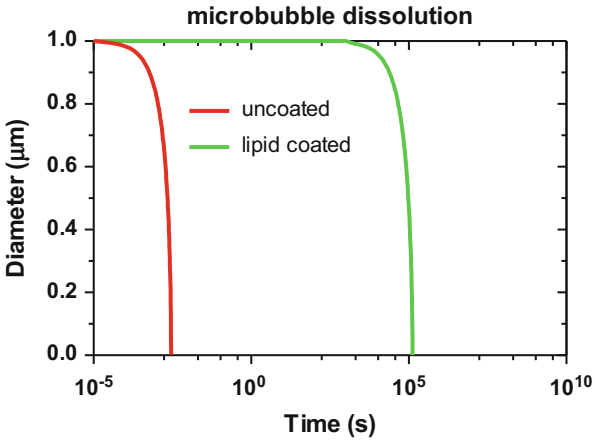

Fig. 2 Microbubble dissolution curves in air-saturated media. The uncoated microbubble dissolution curve (*red*) was calculated using Eq. 2 with $L = 0.02, D = 2 \times 10^{-5}$ cm^2/s, $\sigma = 73$ mN/m, $P_0 = 10^5$ Pa, and $f = 1$. The lipid-coated microbubble dissolution curve (*green*) was calculated using Eq. 5, with $L = 0.02, D = 2 \times 10^{-5}$ cm^2/s, $\sigma = 3 \times 10^{-4}$ mN/m, $P_0 = 10^5$ Pa, $f = 1$, and $R_{\text{shell}} = 10^3$ s/cm

$$\sigma > \Delta\rho g R^2 \tag{4}$$

For a 1.0-μm-diameter lipid-coated air bubble in water, this gives a lower limit of $\sim 3 \times 10^{-6}$ mN/m. It is interesting to note that ~10-μm-diameter lipid-coated air bubbles have been observed to flatten out during dissolution in unsaturated aqueous media [18], indicating that the surface tension of the lipid monolayer coating may become *less than* $\sim 3 \times 10^{-4}$ mN/m under compression. Both of these values are extremely low and would hardly drive the microbubble to dissolve very fast. The fugacity difference of the gas molecules in the bubble and medium at this low surface tension would be only ~0.1 Pa. Thus, the gas core may be strictly thermodynamically unstable, but the chemical potential gradient is very small.

The lipid monolayer also imposes an additional resistance to gas diffusion ($R_{\text{shell}} \sim 10^3$ s/cm) [19], and this can be modeled by the following equation [18]:

$$-\frac{dR}{dt} = \frac{L}{R_{\text{shell}} + R/D}\left(\frac{1 + 2\sigma/P_0R - f}{1 + 4\sigma/3P_0R}\right) \tag{5}$$

Using the values for σ and R_{shell} imparted by the lipid shell, Eq. 5 predicts that the microbubble will last ~4000 years, an increase over the uncoated microbubble lifetime by eight orders of magnitude! Thus, the lipid-coated microbubble is kinetically trapped against dissolution, owing to the very slow diffusion. Since dissolution is a rate-limiting step in Ostwald ripening, this mechanism would likewise be stalled by the lipid coating.

However, microbubble dissolution is driven not only by the chemical potential gradient of the gas core but also that of the lipid molecules in the monolayer shell. Lee et al. have measured the "equilibrium" surface tension of the lipid monolayer to be ~25 mN/m for lipids above their main phase transition temperature (T_m) [20]. The equilibrium surface tension increases as temperature decreases further and further

below T_m, ultimately approaching the value for a clean air/water interface ($\sigma = 73$ mN/m). This indicates that the lipid molecules are much more closely packed on the microbubble surface than they would be on a flat air/water interface, which reduces their translational entropy. The lipid molecules become packed this way on the microbubble surface during Laplace pressure-driven dissolution. The work used to condense the lipids is provided by the release in free energy as the gas molecules diffuse down their chemical potential gradient. Part of this free energy is stored in the compression state (reduced entropy) of the lipids. The system will tend to thermodynamic equilibrium as this free energy is released by lipids desorbing from the microbubble and reforming hydrated bilayers in the bulk aqueous phase. At present, we do not have a quantitative value of the energy barrier for this desorption process, but it must be rather high, as lipid-coated microbubbles have been observed to be stable over long timescales (at least 1 year in the author's laboratory).

Coalescence is another mechanism to release free energy stored in the microbubbles. Rapid coalescence would lead to thermodynamic equilibrium: complete phase separation of the gas and aqueous phases, where the lipids form bilayer structures within the aqueous phase. Coalescence is inhibited by a hydrated poly (ethylene glycol) (PEG) brush layer, extending away from the microbubble surface. Once the PEG brushes of two approaching microbubbles overlap, a strong steric/osmotic repulsion force arises that opposes the motion [21]. Thus, coalescence is prevented unless the inertia of the colliding bubbles is extremely high, or the approach is extremely slow (i.e., providing enough time to allow PEG-lipids to diffuse out of the contact zone [22]). The thickness of the PEG brush on the microbubble coating has been estimated from self-consistent field (SCF) theory to be ~10 nm [23]. Thus, the onset of this PEG brush-mediated repulsion is expected to occur with ~20 nm separation distance between the microbubble surfaces. It has been found that PEG-lipid is necessary as an "emulsifier" to generate microbubbles; lipid alone will not form a sufficient yield of microbubbles [24].

Lipid Composition and Molecular Structure

The discussion above concludes that two lipid components are necessary to form metastable microbubbles: (1) a main phospholipid species capable of achieving very low surface tension ($\sigma << 1$ mN/m) to inhibit dissolution and/or Ostwald ripening and (2) a PEG-lipid emulsifier capable of forming a hydrated brush of sufficient height and density to inhibit coalescence. Other emulsifiers may be substituted for PEG, but the fact remains that a long-range (tens of nm) repulsion force is necessary to inhibit coalescence over long and short timescales. PEG-lipid is the most common emulsifier used to synthesize microbubbles used in ultrasonics.

The main lipid species is often a saturated diacyl phosphatidylcholine (PC). This molecule has a cylindrical shape and self-assembles via hexagonal packing into planar monolayers and bilayers [11] (Fig. 3a). The cylindrical geometry is ensured by the roughly equivalent diameters of the acyl chains compared to the PC headgroup; the structure of a single acyl chain PC (lyso-lipid) is conical, which

induces curvature and disrupts the planar membrane geometry [25]. Additionally, the extra acyl chain doubles the hydrophobic cavity energy of the lipid molecule, thereby reducing its solubility (critical micelle concentration) by a factor of $e^2 = 7.4$, which helps pin the lipid to the gas/water interface. The fully hydrogenated chains can straighten out in the all-*trans* configuration during packing; a double bond would induce a kink that disrupts lipid packing. The acyl chain length can be manipulated to modulate molecular hydrophobicity and intermolecular van der Waals cohesion forces (Fig. 3a). In fact, PC acyl chain length is perhaps the most valuable molecular parameter for controlling the structure, properties, and performance of microbubbles in ultrasonics applications, as will be discussed throughout this chapter. The lower limit is C16; this is the shortest acyl chain that provides a lipid layer below T_m. PC lipids above T_m typically do not form stable microbubbles. On the other end of the spectrum is C24, which is the longest acyl chain PC lipid that is commercially available currently.

PC typically comprises 80–90 mol% of the lipid monolayer. The overall neutral charge of the PC headgroup limits lateral charge repulsion, allowing the molecules to pack tightly together. PC therefore acts as a monolayer matrix-forming lipid [10]. At the same time, the zwitterionic PC groups interact strongly with water, which is essential for reducing surface energy at the aqueous/lipid interface. The zwitterionic PC surface also is resistant to protein adsorption and opsonization [26], which ultimately helps biomedical performance.

Other lipid headgroups can be substituted for a fraction of PC, such as the negatively charged phosphatidic acid (PA) present in the commercially available ultrasound contrast agent Definity® (Lantheus Medical Imaging). The negative charge can mimic the double layer repulsion of the glycocalyx to minimize undesirable microbubble–cell interactions with red blood cells and endothelium. However, the negative charge can also promote opsonization [26]. On the other hand, positively charged lipid headgroups such as trimethylammonium-propane (TAP) can be used to adsorb negatively charged nucleic acids for gene delivery [27, 28]. These charged lipids rarely exceed 20 mol% of the total lipid owing to lateral charge repulsion that can destabilize the lipid shell, as well as the potential for increased opsonization [26].

The second critical component is the emulsifier, which is typically PEG-lipid (Fig. 3b). The PEG-lipid often comprises 10–20 mol% of the lipid coating. As mentioned above, the PEG-lipid is critical for forming a hydrated brush that inhibits microbubble coalescence. It appears that a PEG molecular weight of at least 2000 Da is necessary to stabilize the microbubbles [29]. At present, PEG molecular weights greater than 5000 Da have not been reported for lipid-coated microbubbles. Longer PEGs may lead to microbubble instability owing to the reduced overall hydrophobicity of the emulsifier molecule, allowing it to desorb more readily, as well as the possibility of a less dense PEG brush. It is also important to keep in mind that the PEG itself is polydisperse – there is a distribution of PEG chain lengths in most commercially available PEG-lipids, although this is rarely quantified with a polydispersity index.

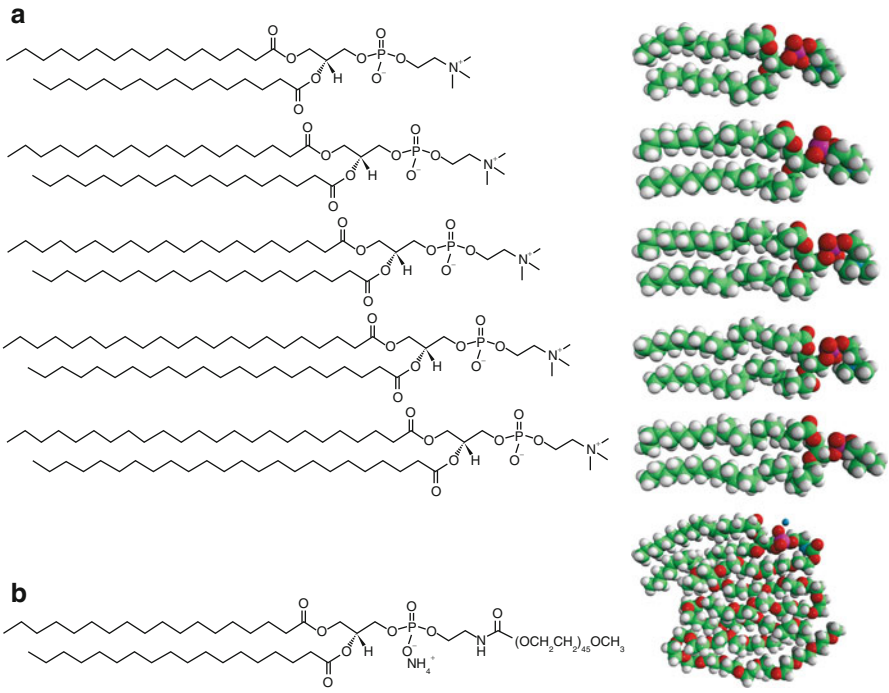

Fig. 3 Molecular structures of lipids commonly used to stabilize microbubbles and nanodrops. (**a**) Saturated diacyl phosphatidylcholine (*PC*) is the main lipid component and often comprises 80–90 mol% of the lipid shell. Shown is the homologous series from C16 to C24. (**b**) poly(ethylene glycol)-lipid serves as an emulsifying agent; shown here is C18 acyl chain length and 2000 Da PEG molecular weight (~45 ethylene oxide mers). These structures were taken from the Avanti Polar Lipids website (http://www.avantilipids.com/)

A secondary advantage of the PEG brush is that it may also inhibit opsonization and unwanted microbubble–cell interactions. On the other hand, the PEG serves as a tether for attaching targeting ligands [24] and nanoparticles [30–32]. Thus, the PEG emulsifier serves as an extremely useful component for more sophisticated microbubble designs.

Microbubble Fabrication

Now that the main lipid components have been identified and their use in microbubble stabilization has been justified, the next step in the rational design paradigm is to investigate processing techniques that lead to various microbubble structures. First, the main techniques to synthesize microbubbles are briefly reviewed. Then, a few postproduction processing steps are reviewed to fine tune and enhance the overall structure.

Microbubble Synthesis

As discussed above, the microbubble is a thermodynamically unfavorable structure. They do not self-assemble; equilibrium favors their disassembly into three separate phases of gas, aqueous medium, and hydrated bilayers. Rather, one must design a process that adds energy to synthesize them and then kinetically traps them in the most desirable state. Three of the more common microbubble fabrication methods are shown schematically in Fig. 4 and discussed in greater detail below.

Sonication

Sonication was the first method described to generate microbubbles for ultrasonics [33]. Sonication involves the high-frequency vibration (typically 20 kHz) of a horn tip at the gas/water interface. This vibration leads to entrainment and secondary breakup through cavitation in the bulk aqueous phase [34, 35]. Unfortunately, there is very little research into the details of bubble entrainment via sonication. It is generally known that low-power sonication with the tip submerged inside the aqueous medium leads to microbubble destruction (clarification) and breakup of the lipid structures from multi-lamellar vesicles (MLVs) into small unilamellar liposomes (SUVs). This is often a preparation step in generating microbubbles. Microbubbles are then generated by moving the probe tip to the gas/water interface and turning the system to full power. Sonication generates many microbubbles very rapidly: for example, 1 L volume of 10^{12}/L can be generated within 1 min. The stochastic processes of entrainment and breakup lead to a fairly polydisperse size distribution, which can be refined using centrifugation steps as outlined below [36]. Thus, sonication is a simple and economical method of generating microbubbles in high yield and admittedly is the preferred method used by the author's research group.

As mentioned above, low-solubility perfluorocarbon gases can be used to decelerate microbubble dissolution. This leads to higher microbubble yields, longer shelf-life, and longer in vivo circulation persistence (i.e., the so-called second-generation ultrasound contrast agents). In sonication, the gas is simply made to flow directly over the aqueous suspension.

A critical step in microbubble generation and stabilization is the adsorption of lipid onto the gas/water interface. This involves shuttling lipid from MLVs or SUVs through the aqueous phase to the newly formed microbubbles. One can model the adsorption process as a chemical reaction involving a particular collision frequency and activation energy. The collision frequency can be increased through increasing lipid concentration (e.g., more SUVs) and convection, which thins the concentration boundary layer. It has been found that 1 mg/mL lipid usually is sufficient to generate a microbubble suspension at 10^9/mL. Since the process necessarily exposes the hydrophobic acyl chains of the lipid molecules to water, there also is an activation energy barrier that limits the kinetics. Lipid adsorption to macroscopic interfaces under static conditions can take minutes or even days. However, as mentioned above, sonication can lead to lipid deposition rates of at least 10 m^2/min and possibly higher. Thus, sonication accelerates the reaction. Microstreaming and acoustic

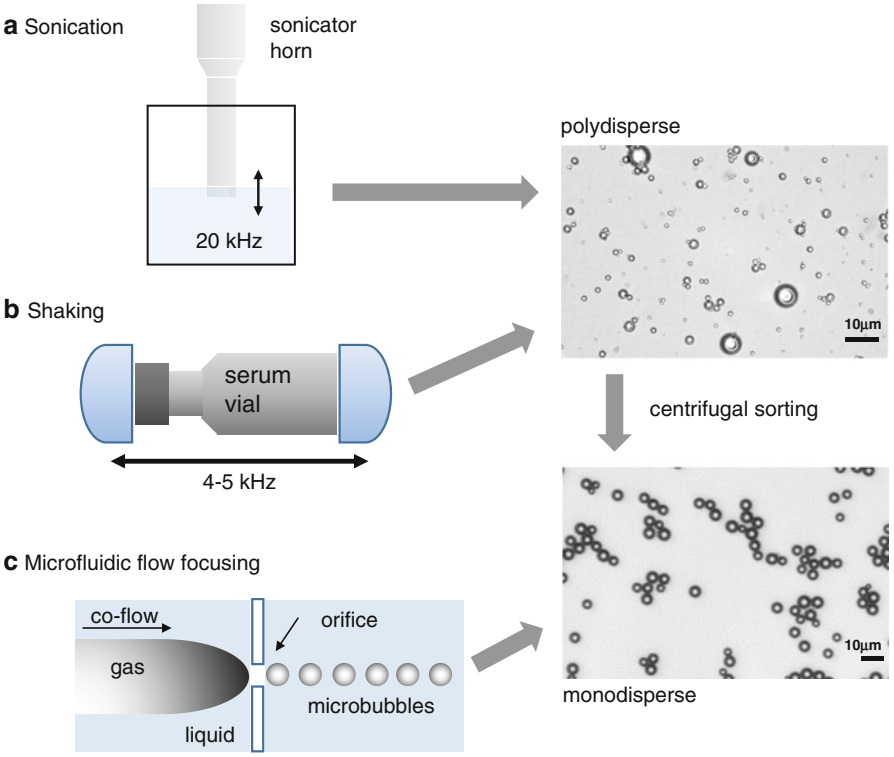

Fig. 4 Methods of microbubble synthesis and centrifugal sorting. Sonication (**a**) and shaking (**b**) produce polydisperse microbubbles very rapidly and economically, but they must be centrifugally sorted to a monodisperse size. Microfluidic methods (**c**) produce monodisperse microbubbles, but at relatively slow rates

radiation forces induce fluid flow that may increase the collision frequency between SUVs and the gas/water interface. Additionally, sonication may catalyze the reaction by highly localized (pico-liter volume) heating events at cavitation sites within the bulk phase. More research is necessary to better understand the bubble formation process during sonication, as well as how the sonication parameters affect microbubble size.

Shaking

Shaking is another process of mechanical agitation that is used to create microbubbles. Typically, a small volume (~1 mL) of lipid solution is sealed in a small vial with a gas headspace and placed in a dental amalgamator or similar mixing device. The device vibrates along the long axis of the vial at ~4000 Hz. This method is used to generate Definity® microbubbles, for example. The benefit of the shaking method is that it can produce microbubbles rapidly (~10^9 in less than one minute) almost anywhere, on demand. The lipid suspension in the vial can be made at a

central facility, sterilized, and then shipped to the end user, who simply places the vial into the shaking device to generate the microbubbles. Thus, it is a very simple and economical method for multiple uses of small quantities of microbubbles. As with sonication, the bubble entrainment and breakup processes during shaking are poorly understood, but it is known that they lead to a polydisperse size distribution. Coincidentally, the size distribution of microbubbles formed by shaking tends to be remarkably similar to that of microbubbles formed by sonication, despite the very different geometry and characteristic frequency. More research is necessary to better understand the bubble formation process during shaking, as well as how the shaking parameters affect the microbubble size.

Microfluidics

More recently, researchers have begun investigating microfluidic techniques to generate microbubbles [37]. This follows advances in the design and fabrication of microfluidic devices, as well as empirical, theoretical, and computational work that has developed correlations to simplify the analysis of fluid mechanics in microfluidic flows. The main phenomenon exploited by microfluidic microbubble generation is flow focusing, in which a thread of gas sheathed by a liquid layer is forced to flow through a contraction and then expansion. The divergent flow leads to a capillary instability that breaks off microbubbles in a very regular pattern, leading to a monodisperse size distribution. The microbubble radius scales with flow rate in a planar flow-focusing device operating at high Reynolds number according to the following equation [38]:

$$\frac{R}{w} \propto \left(\frac{Q_{\text{gas}}}{Q_{\text{liquid}}} \right)^{2/5} \tag{6}$$

where w is the width of the nozzle and Q_{gas} and Q_{liquid} are the flow rates of the gas and liquid streams, respectively ($Q_{\text{liquid}} > Q_{\text{gas}}$). Thus, increasing the flow rate of the gas stream leads to a higher production rate, while increasing the relative flow rate of the liquid stream leads to smaller microbubbles.

The control over microbubble size and the possibility of directed assembly for more sophisticated structures are highly desirable aspects of microfluidic methods. Additionally, the devices are relatively easy to observe during operation with current high-speed imaging techniques, thus providing insight into the physics and engineering of the bubble formation. The main drawback is the relatively low yield (up to $\sim 10^6$/s). Additionally, microfluidic methods are relatively difficult and expensive to employ, as they require clean-room microfabrication facilities to build the device and some trial-and-error tuning and optimization of the relative gas and liquid flows to reproducibly generate the microbubbles. Typically, this is done with expensive microscopy and high-speed camera tools. More research is necessary to better understand the lipid coating process and how to engineer it for more efficient generation of stable microbubbles.

Postproduction Processing

Centrifugal Sorting

As shown below, size is a key structural feature of the microbubble that affects its acoustic properties and biomedical performance. Control of diameter is therefore essential to improving precision in ultrasonic applications employing microbubbles. As mentioned above, size can be controlled during microbubble synthesis with microfluidics by changing the gas and liquid flow rates and nozzle size [38]. However, microfluidics is not the only means of obtaining a monodisperse microbubble suspension. One can take the polydisperse suspensions obtained from sonication or shaking (or any other production method) and subject them to a series of centrifugation steps to isolate microbubbles of a select size [36]. The principle of operation is that microbubbles of different migration speeds under the centrifugal field fractionate into either a "cake" layer at the top or the aqueous subphase below. The migration rate of a microbubble is related to its size by the Stokes rise velocity (u) for low Reynolds number:

$$u = \frac{2\Delta\rho g R^2}{9\mu} \tag{7}$$

where μ is the viscosity of the aqueous phase. Note that the migration speed scales as R^2, which enhances the precision of this technique.

To isolate microbubbles above or below a certain size, one simply defines a cutoff radius and centrifugal strength (g) and then calculates the residence time (t) from the migration rate and height (h) of the centrifuge column (typically a stoppered syringe of 1–10 cm).

$$t = \frac{h}{u} \tag{8}$$

A centrifugal strength of 100–500 RCF (relative centrifugation to Earth's gravitational field) is sufficient to reduce the residence time to a few minutes without inducing an overly destructive hydrostatic pressure (P_0) on the microbubbles (see Eq. 5 above). Equation 7 is valid because viscous drag causes the microbubbles to accelerate and decelerate to the migration speed within a fraction of a second. One important consideration is that the microbubble suspension should be below 20 vol. % to avoid multi-bubble interactions that cause the migration rates to deviate from Eq. 7.

To sort microbubbles by this method, one simply performs multiple centrifugation steps, defining cutoff sizes above and below the desired radius. Microbubbles can be obtained from either the cake or the subphase; the PEG brush layer provides osmotic/steric stability against coalescence within the cake to preserve the size distribution. Once the desired size is isolated, the suspension can be refined by repeating centrifugations until the polydispersity index (the ratio of the volume-weighted mean radius to the number-weighted mean radius) drops to the desired

value. This is typically accomplished within an hour. With sufficient experience, very few microbubbles are lost during this procedure. Combined with sonication, this economical method provides a very high yield of low-polydispersity microbubbles of select size in a relatively short period of time.

Heat Treatment

As shown below, microstructure of the lipid coating can have a significant effect on the microbubble properties. Microstructure arises owing to crystallization of the lipids on the bubble surface to form domains (grains) surrounded by interdomain regions (boundaries) [10, 15]. The crystallization process follows classical nucleation–growth theory and terminates in a polycrystalline shell. Thus, one can use concepts from metallurgy to characterize and engineer the microbubble shell. Initially, crystallization occurs as the surface area is reduced (surface pressure increased) during Laplace pressure-driven dissolution of the newly formed microbubble, until it is stabilized by effectively zero surface tension. Since each microbubble has undergone its own peculiar formation and stabilization history, there may be a strong polydispersity in the microstructures. To improve uniformity and control microstructure, one can heat the microbubble suspension to a temperature above T_m of the main lipid species to melt the coating. One then cools the suspension at a certain rate, allowing the recrystallization. Slow cooling favors growth over nucleation, leading to a smaller number of large domains and therefore a low defect density. Rapid quenching favors nucleation over growth, leading to a larger number of small domains and therefore a high defect density. One can also anneal the polycrystalline shell (fuse the domains) by holding the microbubble suspension to a few degrees just below T_m [15].

Since the lipid coating is at least a binary mixture of phospholipid and emulsifier, there may be phase separation owing to the different nucleation and growth rates of the different species. This has been observed on lipid shells as domains of PC surrounded by interdomain regions of PEG-lipid [16, 29]. Fluorescent membrane dyes often partition with the PEG-lipid in the interdomain region, and the microbubbles appear like soccer balls under the microscope, with dark PC domains surrounded by bright PEG-lipid-enriched regions (Fig. 5).

Additionally, the selection of the PC lipid may influence the domain morphology and therefore defect density. For example, longer chain lipids may be kinetically trapped at high cooling rates as highly ramified dendritic (snowflake) domains, whereas shorter chains lipids may equilibrate to circular cloven domains when subjected to the same heat treatment [16]. More research is necessary to better understand and control the lipid crystallization process and the evolution of domain morphology over time.

Functionalization

Once microbubble size and microstructure of the lipid domains are set, one can further functionalize the microbubble by attaching molecules or nanoparticles to the surface. The simplest method is simple electrostatic adsorption, which can be used in layer-by-layer assembly to build polyelectrolyte multilayer shells [28]. Alternatively,

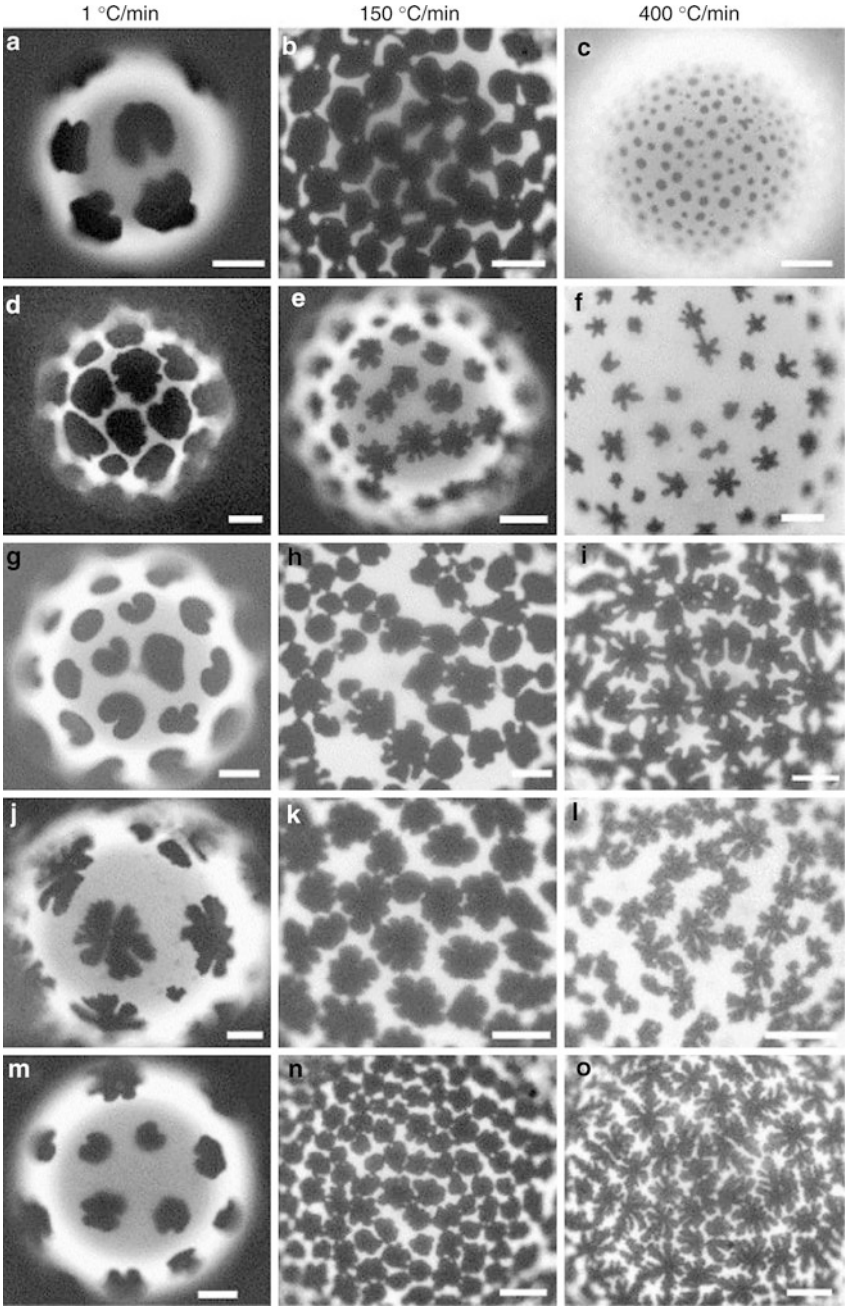

Fig. 5 Fluorescent micrographs of microbubbles heated to melt the lipid coating and then cooled at various rates. The lipid coating comprises a mixture of PEG40S:NBD-PC: (**a**–**c**) di$C_{16:0}$PC, (**d**–**f**) di$C_{18:0}$PC, (**g**–**i**) di$C_{20:0}$PC, (**j**–**l**) di$C_{22:0}$PC, (**m**–**o**) di$C_{24:0}$PC. Scale bars represent 20 μm (Taken from Borden et al. [16])

there are a variety of conjugation chemistries that have been described in the literature [24], including ligand–receptor avidin–biotin and covalent maleimide–thiol coupling. The advantage of these techniques is greater control over the loading density and configuration by virtue of the inherent specificity and stoichiometry of the chemical reactions. More sophisticated ligand expression can be achieved using tiered surface architectures to enhance exposure [39] or concealment [40] of the ligand. Additionally, there are many examples of nanoparticle loading onto microbubbles that have been reported in the literature [31, 41], including polymer, gold and iron oxide nanoparticles, quantum dots, liposomes, lipoplexes, and polyplexes.

Nanodrop Fabrication

Nanodrops are distinct from microbubbles in their size (submicron vs. micron) and the phase state of the interior fluorocarbon phase (liquid vs. gas). Otherwise, they are very similar in the sense that the lipid coating inhibits dissolution and coalescence to stabilize the aqueous emulsions. The nanodrop itself is not very echogenic or acoustically responsive owing to the relative small size and, more importantly, incompressibility of the liquid core. However, the nanodrop can be extremely ultrasound responsive if one can tune the composition and structure such that it vaporizes into a microbubble upon insonation (or some other stimulation). This is the so-called phase-change agent: a microbubble in a more compact form. Most fluorocarbons experience a fivefold change in radius upon vaporization. Thus, a 200-nm-diameter droplet can form a 1-μm-diameter microbubble. The smaller size of the droplets may provide new biomedical performance capabilities that were previously unavailable to microbubbles, such as longer circulation and accumulation in tumors owing to the enhanced permeability and retention effect. Additionally, the vaporization event itself is highly energetic and can be used to facilitate imaging, drug delivery, and ablation.

Two basic methods have been described to form phase-change nanodrops. The first method reported for longer chain fluorocarbons (perfluoropentane and above) was homogenization followed by extrusion [42]. All of the processing occurs with the fluorocarbon in the liquid phase. Unfortunately, however, the more cohesive fluorocarbons require relatively large acoustic energy (mechanical index) to induce a phase transition. More recently, a new method has been described to generate nanodrops of low-boiling fluorocarbons, such as F-propane and F-butane [42]. The method involves first generating a suspension of microbubbles and then cooling and pressurizating the suspension to induce a vapor-to-liquid phase transformation to form nanodrops [43]. The nanodrops are then brought back to standard pressure and temperature, where they remain remarkably metastable in the liquid form to phase change unless they are stimulated by a relatively small acoustic energy (Fig. 6). The superheated drops remain metastable owing to the need for homogenous nucleation and growth of a vapor embryo, making 90 % of the critical temperature the main trigger, rather than the boiling temperature [44]. Yet they can be vaporized acoustically at a clinically relevant mechanical index [45, 46]. One important advantage of

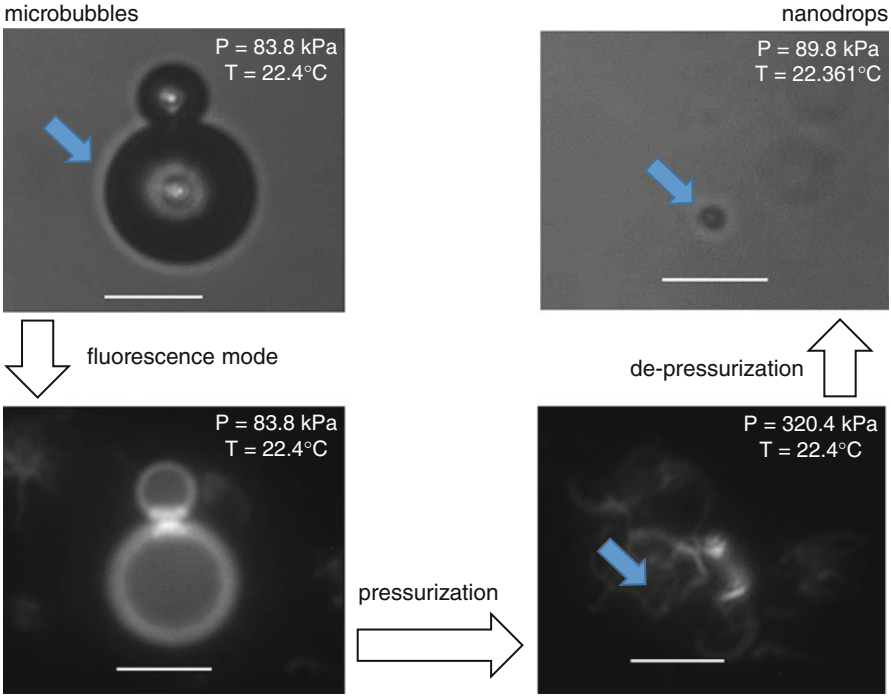

Fig. 6 Nanodrop synthesis by microbubble condensation. A relatively large microbubble (denoted by the *blue arrow*) shown in both bright-field and fluorescent microscopy modes (*left*) is pressurized to form a nanodrop (*bottom right*). Note the shedding of excess fluorescent lipid by this process. Upon depressurization back to standard conditions (*top right*), the nanodrop remains metastable in a superheated state (Images adapted from Mountford et al. [43])

the superheated droplets is the ability to engineer the formulation via control over microbubble composition and microstructure, as described throughout this chapter.

Structure–Property–Performance Relationships

Microbubble Size

Size is a key structural parameter of a microbubble that determines its acoustic properties and biomedical performance. For example, the acoustic response of a microbubble is most intense when driven at the resonance frequency [47]. The linearized eigenfrequency for small-amplitude oscillations of an uncoated microbubble (i.e., the Minnaert frequency) depends on the initial "resting" radius of the microbubble (R_0) according to the following equation [48]:

$$f_0 = \frac{1}{2\pi R_0}\left(\frac{3\gamma P_0}{\rho_0} + \frac{2(3\gamma - 1)\sigma}{\rho_0 R_0}\right)^{1/2} \tag{9}$$

where γ is the ratio of specific heats for the gas inside the bubble, P_0 is the hydrostatic pressure, and ρ_0 is the density of the surrounding aqueous phase. Equation 6 shows that, for an uncoated microbubble, the surface tension term (second term in the brackets) becomes significant as R_0 approaches one micrometer. Thus, the resonance frequency transitions from an ${R_0}^{-1}$ dependence to an ${R_0}^{-3/2}$ dependence as the diameter decreases from 10 to 1 μm. Equation 9 predicts that the resonance frequency increases from 0.7 to 12 MHz as the microbubble diameter decreases from 10 to 1 μm. Thus, we expect that the echogenicity of a microbubble is highly dependent on its size. Indeed, it was found that 1–2-μm-diameter microbubbles provided a negative contrast (attenuation) when imaged in vivo at 40 MHz, while 6–8-μm-diameter microbubbles provided a positive contrast (scattering) under the same conditions [49]. This is partly owing to damping, discussed below. Polydispersity in the microbubble size distribution therefore presents an obstacle for quantitative imaging (e.g., molecular imaging), where it is desirable for the linearized video intensity to increase linearly with microbubble concentration. For contrast-enhanced ultrasound imaging, it is thus desirable to start with a microbubble suspension of uniform size matched to the resonance frequency of the ultrasound device.

The microbubble interaction volume scales as $R_{\max}^3$, where $R_{\max}$ is the maximum radius experienced by the microbubble during an acoustically driven oscillation. Even when considering nonlinear bubble oscillations, $R_{\max}$ scales with R_0. According to the Marmottant model, for example, a 6-μm-diameter microbubble has an $R_{\max}$ value of 9.6 μm when driven at 1 MHz and 0.5 MPa peak negative pressure, whereas a 2-μm-diameter microbubble has an $R_{\max}$ value of 6.6 μm under the same conditions [50]. Thus, microbubble size is expected to significantly impact therapeutic efficiency. Indeed, larger microbubbles were observed to be more effective in vivo at blood–brain barrier (BBB) opening [51].

Microbubble size also affects microbubble stability and pharmacodynamics. As can be seen from Eq. 5, the dissolution rate increases with decreasing microbubble radius owing to the greater Laplace pressure, greater surface area-to-volume ratio, and a thinner concentration boundary layer; thus smaller microbubbles dissolve faster than larger ones. Indeed, smaller microbubbles were also observed to be more susceptible to destruction by fragmentation under acoustic stimulation [52]. Additionally, it has been found that larger microbubbles circulate in vivo much longer than smaller microbubbles [49].

Lipid Shell Elasticity

The elastic properties of the lipid coating can significantly affect the resonance frequency of the microbubble. The surface elasticity (χ) of a lipid monolayer is defined as [50]:

$$\chi = A\left(\frac{d\sigma}{dA}\right) \tag{10}$$

where A is the monolayer area and σ is the surface tension, as above. The linearized eigenfrequency of a lipid-coated microbubble with a shell elasticity undergoing small-amplitude oscillations (where $\sigma = 0$ at R_0, as shown above) is given by the following equation [53]:

$$f_0 = \frac{1}{2\pi R_0}\left(\frac{3\gamma P_0}{\rho_0} + \frac{4\chi}{\rho_0 R_0}\right)^{1/2} \tag{11}$$

Typical values of the lipid monolayer shell elasticity have been measured to be 0.5–1.0 N/m [53, 54]. Under these conditions, the shell term (second term in the brackets) dominates as R_0 approaches one micrometer, and the resonance frequency increases as ${R_0}^{-3/2}$. Experimental measurements have shown that the resonance frequency of a lipid-coated microbubble increases from 1 to 10 MHz as the diameter decreases from 10 to 1 μm [48]. It should be noted that microbubbles driven to large-amplitude oscillations deviate from Eq. 11 owing to shell rupture and buckling [50], which are not captured by the linearized model.

Elasticity of the lipid coating may affect not only the acoustic response but also the stability and pharmacodynamics of microbubbles. Sarkar et al. predicted that lipid shell elasticity may affect microbubble stability by resisting monolayer expansion and compression [55]. For example, elasticity of the lipid coating may explain the remarkable stability of small diameter (1–2 μm) microbubbles [56]. Experiments have confirmed that the lipid coating does have a significant effect on the growth and dissolution of a microbubble during gas exchange, and elasticity appears to be a function of both lipid composition and domain microstructure [57]. More research is necessary to better establish the effects of lipid composition and microstructure on shell elasticity and the exploitation of shell elasticity to achieve higher levels of performance in ultrasound applications.

Lipid Shell Viscosity

The surface viscosity of the lipid coating can affect the acoustic response and other properties of the microbubble. DH Kim et al. showed that lipid composition and microstructure have a profound effect on the surface shear yield and surface shear viscosity (η_s) of lipid-coated microbubbles [15]. The surface shear viscosity is expected to affect lipid buckling and folding during compression, thus altering stability. It was shown that increasing η_s (i.e., in-plane rigidity) by increasing phospholipid acyl chain length can cause a corresponding increase in microbubble stability against dissolution, acoustic destruction, and contrast agent half-life [58].

Additionally, the surface dilatational viscosity (κ_s) can affect microbubble expansion and is modeled to affect both expansion and contraction during oscillations under ultrasound stimulation. The linearized damping term for the microbubble shell is given by [53]:

$$\delta_{\text{shell}} = \frac{4\kappa_s}{2\pi f_0 \rho R_0^3} \tag{12}$$

The shell damping term is a part of the overall damping coefficient:

$$\delta = \delta_{\text{shell}} + \delta_{\text{rad}} + \delta_{\text{visc}} \tag{13}$$

where δ_{rad} and δ_{visc} are the damping coefficients corresponding to acoustic reradiation and viscous dissipation of the aqueous phase, respectively. These terms are given by [53]:

$$\delta_{\text{rad}} = \frac{2\pi f_0 R_0}{c} \tag{14}$$

$$\delta_{\text{vis}} = \frac{2\mu}{\pi \rho f_0 R_0^2} \tag{15}$$

where c is the speed of sound in aqueous media. Note that all of the damping terms depend on microbubble size, again pointing to the importance of monodispersity for more precise acoustics. The resonance frequency deviates from the eigenfrequency according to the following relationship [53]:

$$f_r = f_0 \sqrt{1 - \frac{\delta^2}{2}} \tag{16}$$

The effect of lipid shell damping on the resonance frequency is rather small [53]; however, damping does effect the ratio of acoustic energy that is either scattered or attenuated (lost to heat dissipation). This explains the result mentioned above that smaller microbubbles can provide negative contrast, while larger microbubbles provide positive contrast for in vivo imaging at 40 MHz [49]. Damping also affects the lifetime of the signal (ring down) after the termination of the ultrasound pulse. Additionally, damping affects how much energy is converted from the acoustic wave to the local microenvironment by the microbubble, thus affecting therapeutic applications such as sonoporation and thermal ablation. Microbubble shell damping is an important property, but very little is known about the molecular mechanisms and microstructural effects of lipid monolayer rigidity and friction, particularly on microbubble shells. More research is needed to unravel these interrelationships and to put this knowledge to practice for advanced acoustic applications.

Viscoelastic Effects on Microbubble Stability

Sarkar et al. showed theoretically that viscoelasticity of the lipid monolayer shell can have a profound effect on microbubble stability [55]. Since changes in microbubble surface area are relatively slow for dissolution compared to ultrasonic oscillations, the

surface viscosity term often is assumed to have a negligible effect on microbubble stability. The surface elasticity, however, is expected to contribute significantly to microbubbles stability. In Sarkar's model, the elasticity resists both compression and expansion of the surface beyond the equilibrium state (equilibrium surface tension) of the phospholipid shell. Sarkar estimated, for example, an increase in the ratio of elasticity to the equilibrium surface tension (χ/σ_0) from 1.0 to 20 can increase the lifetime of a 2.5-μm-diameter air bubble from complete dissolution in ~20 s to almost no dissolution over 10^3 s [55]. Additionally, elasticity can explain the very long lifetimes observed for individual microbubbles. Sarkar estimated, for example, that an increase of χ/σ_0 from 1.0 to 1.05 was sufficient to explain the indefinite stability of submicron bubbles.

However, experimental data on microbubble growth and dissolution during gas exchange have indicated that the true situation for surface elasticity is much more complex than even the more advanced elasticity models employed by Sarkar [55, 59, 60]. In his doctoral dissertation experiment, JJ Kwan started with an SF_6 gas-filled microbubble suspended in an SF_6-saturated aqueous medium and then suddenly replaced the medium with air-saturated fluid. The microbubble was held in place with a hollow cellulose microfiber (dialysis tubing), which is highly permeable to dissolved gases, during the exchange of medium [61]. The medium exchange was ensured by using a low-volume, laminar-flow perfusion chamber. The microbubble was viewed under bright-field microscopy during the gas exchange process. Image analysis of the captured video frames was used to generate radius–time curves. Interestingly, the microbubble was found to initially grow owing to the influx of much faster diffusing and more soluble O_2 and N_2. Once the partial pressures equalized, the microbubble shank with the efflux of SF_6 (which was absent in the surrounding medium). The microbubble stopped shrinking near its initial radius. It then remained stable for some time before again dissolving to a smaller diameter (typically ~1–2 μm). These experimental radius–time curves were compared to predictions from a theoretical model that accounted for mass transport of each gas species to and from the microbubble. The model had been previously validated with Kwan's experimental setup by comparing growth and dissolution curves for the soluble surfactant sodium dodecyl sulfate (SDS) [61]. To fit the radius–time curves for lipid-coated microbubbles, the "apparent" surface tension was varied for each time step. The surface tension was then plotted as a function of microbubble surface area to determine the stress–strain relationships [57].

The resulting surface tension-area isotherms showed very complex elastic behavior. During the initial microbubble growth phase, the surface tension increased linearly with area, indicating a linear elastic regime. This linear behavior continued from essentially zero surface tension to a surface tension approaching ~72 mN/m, the surface tension of a clean air/water interface. Remarkably, the surface tension then started to decrease exponentially to 25 mN/m (curiously close to the equilibrium surface tension of a liquid expanded-phase phospholipid monolayer [20]), even as the microbubble continued to grow! Finally, during subsequent microbubble compression, the surface tension was found to decrease from 25 mN/m back to ~0 mN/m as the bubble approached its initial diameter. The decrease in surface tension appeared to be a linear function of area, but the slope (and therefore elasticity) was much lower than that found for the expansion phase. Thus, there is significant hysteresis between the expansion and compression curves.

The following sequence of microstructural events were used to explain this highly nonlinear elastic behavior: (1) the lipid monolayer expands elastically from the resting state to rupture; (2) the monolayer ruptures into domains (islands) of condensed lipids, which slowly dissolve to fill in the vacuum of free gas/water interface between the domains; (4) upon compression, the lipids repack into domains; and (5) the domains repack and halt dissolution at the initial, resting surface area. The latter step is a remarkable self-healing phenomenon. This explanation was supported by Langmuir trough data of phospholipid monolayers slowly compressed to the collapse plateau and then suddenly expanded. Taken together, these data show that the lipid shell elasticity depends highly on its particular microstructure, which in turn depends on the composition and processing history of the individual microbubble. Similar behavior is expected for lipid-coated, liquid-filled fluorocarbon nanodrops.

Lipid Shell Permeability

Microbubble stability is not solely governed by the lipid shell elasticity. Another property that affects the rate and extent of microbubble growth and dissolution is the monolayer permeability to gases. As mentioned above, prior experimental evidence showed that the lipid shell can impede oxygen transport [19]. This was shown using an ultra-microelectrode (UME) juxtaposed to a microbubble held by a micropipette. Voltage applied to the UME induced the reduction of dissolved oxygen in a diffusion-limited process, which induced oxygen release and transport from the nearby microbubble. The reaction rate could be monitored by following the current applied to the UME. A simple mass transport model was used to back out the permeability of the lipid monolayer shell from the steady-state current at each UME-microbubble separation distance. It was found that the lipid monolayer permeation resistance increased exponentially with increasing phospholipid acyl chain length, which confirmed prior work by VK La Mer and colleagues with fatty acids and alcohols on retardation of water evaporation [62]. La Mer favored an energy barrier model for monolayer permeation, in which it was predicted that increasing lipid hydrophobic chain length would lead to a greater activation energy owing to a deeper van der Waals intermolecular potential well. In other words, a smaller fraction of the gas molecules colliding with the monolayer had enough kinetic energy to punch through, according to the Boltzmann distribution, thus inhibiting gas transport. The effect of the lipid shell permeability on gas transport has also been modeled by Sarkar et al. [63, 64]. Again, similar effects are expected for lipid-coated, fluorocarbon liquid-filled nanodrops.

Conclusion and Future Directions

Over a decade ago, DH Kim first described the materials science paradigm of composition → processing → structure → property → performance for rational design of lipid-coated microbubbles. Since then, a significant body of work has

elucidated the effects of composition and processing on microbubble structure, as well as some structure–property–performance relationships. For example, only after centrifugal sorting to control size had been mastered was it possible to show that longer acyl chain lipids lead to better microbubble stability, acoustic longevity, and in vivo circulation persistence.

However, more research is necessary to fully unlock the mystery of how lipid composition and processing affect lipid domain microstructure. Moreover, it is important to further establish the interrelationships between lipid shell microstructure and key microbubble physical properties, such as the shell elasticity and viscosity. For example, the molecular mechanism for lipid shell friction must be elucidated, so that we can better avoid or exploit acoustic damping effects on microbubble performance in ultrasound imaging and therapy. Ultimately, greater flexibility and control over the lipid coating microstructure coupled with a better understanding of key microbubble structure–property relationships will enable true innovations in biomedical ultrasound.

References

1. Borden MA (2014) Microbubble dispersions of natural lung surfactant. Curr Opin Colloid Interface Sci 19(5):480–489
2. McCulley JP, Shine WE (2001) The lipid layer: the outer surface of the ocular surface tear film. Biosci Rep 21(4):407–418
3. Goldberg BB, Liu J-B, Forsberg F (1994) Ultrasound contrast agents: a review. Ultrasound Med Biol 20(4):319–333
4. de Jong N, Ten Cate FJ, Lancée CT, Roelandt JRTC, Bom N (1991) Principles and recent developments in ultrasound contrast agents. Ultrasonics 29(4):324–330
5. Stride E, Saffari N (2003) Microbubble ultrasound contrast agents: a review. Proc Inst Mech Eng H 217(6):429–447
6. Lindner JR (2004) Microbubbles in medical imaging: current applications and future directions. Nat Rev Drug Discov 3(6):527–533
7. Wilson SR, Burns PN (2010) Microbubble-enhanced US in body imaging: what role? Radiology 257(1):24–39
8. Dayton PA, Rychak JJ (2007) Molecular ultrasound imaging using microbubble contrast agents. Front Biosci J Virtual Libr 12:5124–5142
9. Ferrara K, Pollard R, Borden M (2007) Ultrasound microbubble contrast agents: fundamentals and application to gene and drug delivery. Annu Rev Biomed Eng 9:415–447
10. Kim DH. Mechanical properties, microstructure, and specific adhesion of phospholipid monolayer-coated microbubbles. Thesis PhD DUKE Univ Source DAI-B 6101 P 471 Jul 2000 177 Pages [Internet]. 1999 Oct [cited 2015 May 22]; Available from http://adsabs.harvard.edu/abs/1999PhDT.....87K
11. Israelachvili JN (2010) Intermolecular and surface forces. Academic, San Diego, 706 p
12. Prausnitz JM, Lichtenthaler RN, de Azevedo EG (1998) Molecular thermodynamics of fluid-phase equilibria. Pearson Education, New Jersey, 1245 p
13. Epstein PS, Plesset MS (1950) On the stability of gas bubbles in liquid-gas solutions. J Chem Phys 18(11):1505–1509
14. Duncan PB, Needham D (2004) Test of the Epstein-Plesset model for gas microparticle dissolution in aqueous media: effect of surface tension and gas undersaturation in solution. Langmuir 20(7):2567–2578

15. Kim DH, Costello MJ, Duncan PB, Needham D (2003) Mechanical properties and microstructure of polycrystalline phospholipid monolayer shells: novel solid microparticles. Langmuir 19(20):8455–8466
16. Borden MA, Pu G, Runner GJ, Longo ML (2004) Surface phase behavior and microstructure of lipid/PEG-emulsifier monolayer-coated microbubbles. Colloids Surf B Biointerfaces 35(3-4):209–223
17. Witten TA, Wang J, Pocivavsek L, Lee KYC (2010) Wilhelmy plate artifacts in elastic monolayers. J Chem Phys 132(4):046102
18. Borden MA, Longo ML (2002) Dissolution behavior of lipid monolayer-coated, air-filled microbubbles: effect of lipid hydrophobic chain length. Langmuir 18(24):9225–9233
19. Borden MA, Longo ML (2004) Oxygen permeability of fully condensed lipid monolayers. J Phys Chem B 108(19):6009–6016
20. Lee S, Kim DH, Needham D (2001) Equilibrium and dynamic interfacial tension measurements at microscopic interfaces using a micropipet technique. 2. Dynamics of phospholipid monolayer formation and equilibrium tensions at the water-air interface. Langmuir 17(18):5544–5550
21. Kuhl TL, Leckband DE, Lasic DD, Israelachvili JN (1994) Modulation of interaction forces between bilayers exposing short-chained ethylene oxide headgroups. Biophys J 66(5): 1479–1488
22. Orozco-Alcaraz R, Kuhl TL (2012) Impact of membrane fluidity on steric stabilization by lipopolymers. Langmuir 28(19):7470–7475
23. Chen CC, Borden MA (2011) The role of poly(ethylene glycol) brush architecture in complement activation on targeted microbubble surfaces. Biomaterials 32(27):6579–6587
24. Klibanov AL (2005) Ligand-carrying gas-filled microbubbles: ultrasound contrast agents for targeted molecular imaging. Bioconjug Chem 16(1):9–17
25. Dressaire E, Bee R, Bell DC, Lips A, Stone HA (2008) Interfacial polygonal nanopatterning of stable microbubbles. Science 320(5880):1198–1201
26. Malmsten M (1995) Protein adsorption at phospholipid surfaces. J Colloid Interface Sci 172(1):106–115
27. Christiansen JP, French BA, Klibanov AL, Kaul S, Lindner JR (2003) Targeted tissue transfection with ultrasound destruction of plasmid-bearing cationic microbubbles. Ultrasound Med Biol 29(12):1759–1767
28. Borden MA, Caskey CF, Little E, Gillies RJ, Ferrara KW (2007) DNA and polylysine adsorption and multilayer construction onto cationic lipid-coated microbubbles. Langmuir 23(18):9401–9408
29. Borden MA, Martinez GV, Ricker J, Tsvetkova N, Longo M, Gillies RJ et al (2006) Lateral phase separation in lipid-coated microbubbles. Langmuir 22(9):4291–4297
30. Lum AFH, Borden MA, Dayton PA, Kruse DE, Simon SI, Ferrara KW (2006) Ultrasound radiation force enables targeted deposition of model drug carriers loaded on microbubbles. J Control Release 111(1-2):128–134
31. Lentacker I, Smedt SCD, Sanders NN (2009) Drug loaded microbubble design for ultrasound triggered delivery. Soft Matter 5(11):2161–2170
32. Dove JD, Murray TW, Borden MA (2013) Enhanced photoacoustic response with plasmonic nanoparticle-templated microbubbles. Soft Matter 9(32):7743–7750
33. Feinstein SB, Ten Cate FJ, Zwehl W, Ong K, Maurer G, Tei C et al (1984) Two-dimensional contrast echocardiography. I. In vitro development and quantitative analysis of echo contrast agents. J Am Coll Cardiol 3(1):14–20
34. Li MK, Fogler HS (1978) Acoustic emulsification. Part 1. The instability of the oil-water interface to form the initial droplets. J Fluid Mech 88(03):499–511
35. Li MK, Fogler HS (1978) Acoustic emulsification. Part 2. Breakup of the large primary oil droplets in a water medium. J Fluid Mech 88(03):513–528
36. Feshitan JA, Chen CC, Kwan JJ, Borden MA (2009) Microbubble size isolation by differential centrifugation. J Colloid Interface Sci 329(2):316–324

37. Talu E (2007) Lipid-stabilized monodisperse microbubbles produced by flow focusing for use as ultrasound contrast agents and targeted drug delivery. ProQuest. 127 p
38. Gañán-Calvo AM, Gordillo JM (2001) Perfectly monodisperse microbubbling by capillary flow focusing. Phys Rev Lett 87(27):274501
39. Kim DH, Klibanov AL, Needham D (2000) The influence of tiered layers of surface-grafted poly(ethylene glycol) on receptor-ligand-mediated adhesion between phospholipid monolayer-stabilized microbubbles and coated glass beads. Langmuir 16(6):2808–2817
40. Borden MA, Sarantos MR, Stieger SM, Simon SI, Ferrara KW, Dayton PA (2006) Ultrasound radiation force modulates ligand availability on targeted contrast agents. Mol Imaging 5(3):139–147
41. Sirsi SR, Borden MA (2014) State-of-the-art materials for ultrasound-triggered drug delivery. Adv Drug Deliv Rev 72:3–14
42. Sheeran PS, Luois S, Dayton PA, Matsunaga TO (2011) Formulation and acoustic studies of a new phase-shift agent for diagnostic and therapeutic ultrasound. Langmuir 27(17): 10412–10420
43. Mountford PA, Sirsi SR, Borden MA (2014) Condensation phase diagrams for lipid-coated perfluorobutane microbubbles. Langmuir 30(21):6209–6218
44. Mountford PA, Thomas AN, Borden MA (2015) Thermal activation of superheated lipid-coated perfluorocarbon drops. Langmuir 31(16):4627–4634
45. Sheeran PS, Wong VP, Luois S, McFarland RJ, Ross WD, Feingold S et al (2011) Decafluorobutane as a phase-change contrast agent for low-energy extravascular ultrasonic imaging. Ultrasound Med Biol 37(9):1518–1530
46. Sheeran PS, Luois SH, Mullin LB, Matsunaga TO, Dayton PA (2012) Design of ultrasonically-activatable nanoparticles using low boiling point perfluorocarbons. Biomaterials 33(11): 3262–3269
47. Hoff L (2013) Acoustic characterization of contrast agents for medical ultrasound imaging. Springer, New Jersey, 218 p
48. Doinikov AA, Haac JF, Dayton PA (2009) Resonance frequencies of lipid-shelled microbubbles in the regime of nonlinear oscillations. Ultrasonics 49(2):263–268
49. Sirsi S, Feshitan J, Kwan J, Homma S, Borden M (2010) Effect of microbubble size on fundamental mode high frequency ultrasound imaging in mice. Ultrasound Med Biol 36(6):935–948
50. Marmottant P, van der Meer S, Emmer M, Versluis M, de Jong N, Hilgenfeldt S et al (2005) A model for large amplitude oscillations of coated bubbles accounting for buckling and rupture. J Acoust Soc Am 118(6):3499–3505
51. Choi JJ, Feshitan JA, Baseri B, Wang S, Tung Y-S, Borden MA et al (2010) Microbubble-size dependence of focused ultrasound-induced blood-brain barrier opening in mice in vivo. IEEE Trans Biomed Eng 57(1):145–154
52. Chomas JE, Dayton P, May D, Ferrara K (2001) Threshold of fragmentation for ultrasonic contrast agents. J Biomed Opt 6(2):141–150
53. van der Meer SM, Dollet B, Voormolen MM, Chin CT, Bouakaz A, de Jong N et al (2007) Microbubble spectroscopy of ultrasound contrast agents. J Acoust Soc Am 121(1):648–656
54. Dove JD, Borden MA, Murray TW (2014) Optically induced resonance of nanoparticle-loaded microbubbles. Opt Lett 39(13):3732
55. Katiyar A, Sarkar K, Jain P (2009) Effects of encapsulation elasticity on the stability of an encapsulated microbubble. J Colloid Interface Sci 336(2):519–525
56. Kwan JJ, Borden MA (2012) Lipid monolayer collapse and microbubble stability. Adv Colloid Interface Sci 183–184:82–99
57. Kwan JJ, Borden MA (2012) Lipid monolayer dilatational mechanics during microbubble gas exchange. Soft Matter 8(17):4756–4766
58. Garg S, Thomas AA, Borden MA (2013) The effect of lipid monolayer in-plane rigidity on in vivo microbubble circulation persistence. Biomaterials 34(28):6862–6870

59. Chatterjee D, Sarkar K (2003) A Newtonian rheological model for the interface of microbubble contrast agents. Ultrasound Med Biol 29(12):1749–1757
60. Sarkar K, Shi WT, Chatterjee D, Forsberg F (2005) Characterization of ultrasound contrast microbubbles using in vitro experiments and viscous and viscoelastic interface models for encapsulation. J Acoust Soc Am 118(1):539–550
61. Kwan JJ, Borden MA (2010) Microbubble dissolution in a multigas environment. Langmuir 26(9):6542–6548
62. Mer VKL (2014) Retardation of evaporation by monolayers: transport processes. Academic, New York, 298 p
63. Sarkar K, Katiyar A, Jain P (2009) Growth and dissolution of an encapsulated contrast microbubble: effects of encapsulation permeability. Ultrasound Med Biol 35(8):1385
64. Katiyar A, Sarkar K (2010) Stability analysis of an encapsulated microbubble against gas diffusion. J Colloid Interface Sci 343(1):42–47